Glycerol binding at the narrow channel of photosystem II stabilizes the low-spin S_2 state of the oxygen-evolving complex

David A. Flesher[1, †], Jinchan Liu[1, †], Jessica M. Wiwczar[1, †], Krystle Reiss[2], Ke R. Yang[2], Jimin Wang[1], Mikhail Askerka[2], Christopher J. Gisriel[2], Victor S. Batista[2], and Gary W. Brudvig[1,2,*]

[1]Department of Molecular Biophysics and Biochemistry, Yale University, New Haven, CT 06520, USA.
[2]Department of Chemistry, Yale University, New Haven, CT 05620, USA.
[†]These authors contributed equally.
*To whom correspondence should be addressed: gary.brudvig@yale.edu

Abstract

The oxygen-evolving complex (OEC) of photosystem II (PSII) cycles through redox intermediate states S_i (i = 0 - 4) during the photochemical oxidation of water. The S_2 state involves an equilibrium of two isomers including the low-spin S_2 (LS-S_2) state with its characteristic electron paramagnetic resonance (EPR) multiline signal centered at g = 2.0, and a high-spin S_2 (HS-S_2) state with its g = 4.1 EPR signal. The relative intensities of the two EPR signals change under experimental conditions that shift the HS-S_2/LS-S_2 state equilibrium. Here, we analyze the effect of glycerol on the relative stability of the LS-S_2 and HS-S_2 states when bound at the narrow channel of PSII, as reported in an X-ray crystal structure of cyanobacterial PSII. Our quantum mechanics/molecular mechanics (QM/MM) hybrid models of cyanobacterial PSII show that the glycerol molecule perturbs the hydrogen-bond network in the narrow channel, increasing the pK_a of D1-Asp61 and stabilizing the LS-S_2 state relative to the HS-S_2 state. The reported results are consistent with the absence of the HS-S_2 state EPR signal in native cyanobacterial PSII EPR spectra and suggest that the narrow water channel hydrogen-bond network regulates the relative stability of OEC catalytic intermediates during water oxidation.

Keywords: Electron paramagnetic resonance, glycerol, hydrogen-bond network, oxygen evolution, photosystem II, quantum mechanics/molecular mechanics, S_2 state

Introduction

The oxygen-evolving complex (OEC) is the metallocofactor in photosystem II (PSII) that catalyzes water oxidation, producing molecular oxygen and sustaining life on Earth (Blankenship 2021). The OEC is a cluster of four μ-oxo-bridged Mn ions and a Ca ion (Mn_4CaO_5) embedded in the lumenal side of PSII (Fig. 1). The OEC performs water oxidation through a cycle of redox intermediates known as the Kok cycle (Kok et al. 1970) where oxidizing equivalents are accumulated step-wise in S_i "storage" states (i = 0 - 4), gradually increasing the Mn oxidation states. The transient S_4 state uses the accumulated oxidized equivalents and substrate waters to form an O−O bond, releasing molecular oxygen and resetting the Mn oxidation states to the S_0 state. The structure and function of the OEC have been studied both experimentally (Hillier and Wydrzynski 2000) and theoretically (Sproviero et al. 2008) with reviews reported by Shen (2015) and Vinyard and Brudvig (2017). Nearby the OEC are water channels that act as ingress/egress pathways for water and/or protons (Sproviero et al. 2008; Vogt et al. 2015; Takaoka et al. 2016;

Kaur et al. 2021), one of which is the narrow channel that terminates near O4 of the OEC and can bind glycerol, as we discuss below (Fig. 1).

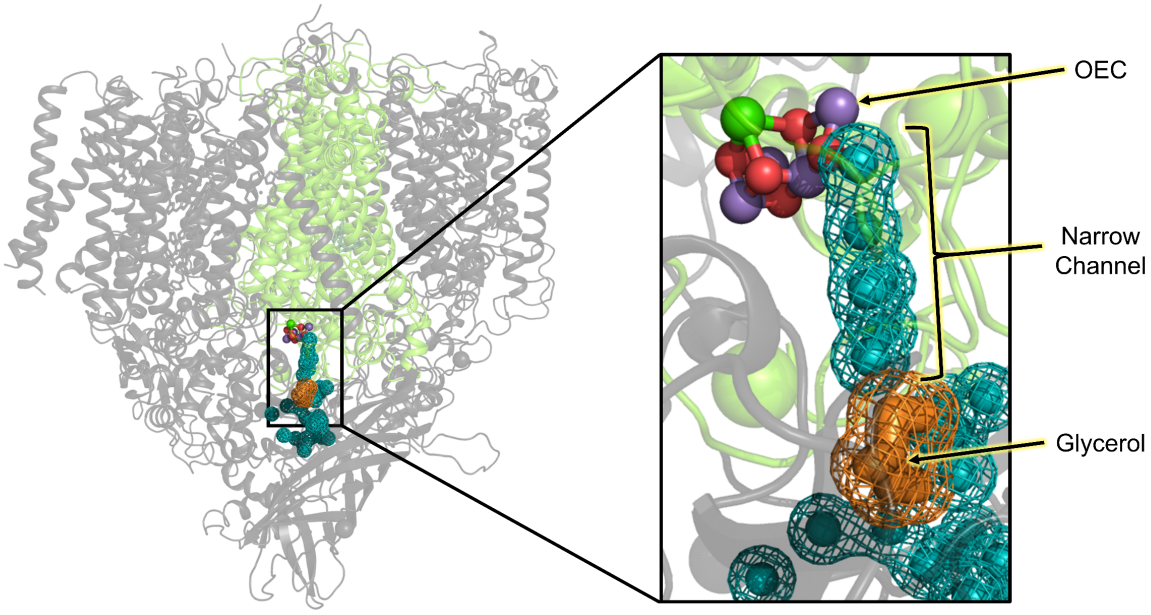

Fig. 1 Left: Membrane plane view of a PSII monomer (PDB 5V2C) with the D1 and D2 subunits shown in light green with all other subunits shown in grey. Right: The OEC is shown as a ball and stick model. The narrow channel is teal and is shown as a mesh surface with modeled waters shown as spheres. The glycerol bound to the narrow channel is orange and is shown as sticks and a mesh surface.

The S_2 state has a long history of study in part due to its reliable experimental isolation and detectable EPR signal (Dismukes and Siderer 1980; Brudvig et al. 1983; Zimmermann and Rutherford 1984). It is comprised of three Mn(IV) ions and one Mn(III) ion and has been modeled as an equilibrium of two isomers: a high-spin S = 5/2 state (HS-S_2) and a low-spin S = 1/2 state (LS-S_2) which shift the position of the Mn(III) ion from Mn4 to Mn1, respectively (Fig. 2). In spinach PSII membranes, these isomers produce distinct EPR signals with the HS-S_2 state producing a broad, featureless peak centered at g = 4.1 while the LS-S_2 state produces a multiline signal centered at g = 2.0 (Fig. 2). Native cyanobacterial PSII only produces the LS-S_2 signal (Fig. 2); however, certain experimental conditions have produced EPR signals similar to the HS-S_2 state (Boussac et al. 2015; Boussac 2019).

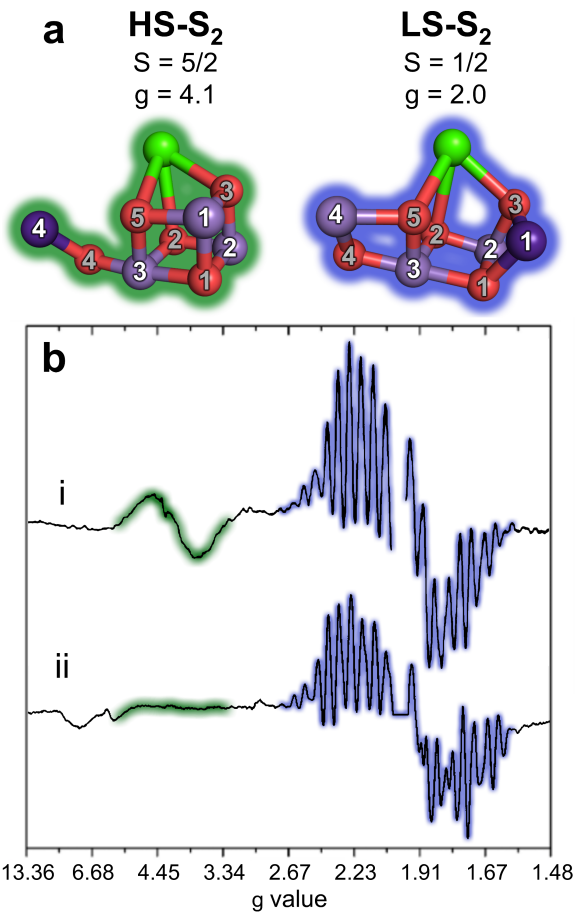

Fig. 2 a Models of the HS-S_2 and LS-S_2 isomers of the OEC shown as closed and open cubane structural isomers, respectively (Pantazis et al. 2012). The Mn and oxygen atoms in the OEC, shown as purple and red spheres, respectively, are labeled according to their position (Mn1-4, O1-5). The oxidation state of each Mn is color coded with Mn(III) colored dark purple and Mn(IV) colored light purple. **b** EPR spectra of the S_2 state. Scan i is from spinach PSII membranes in sucrose-containing buffer, adapted from Pokhrel and Brudvig (2014). Scan ii is from wild-type cyanobacterial PSII purified using glycerol-containing buffers, adapted from Boussac et al. (1998). The region corresponding to the HS-S_2 state signal is highlighted in green and that for the LS-S_2 state in blue to match the outline of the HS-S_2 and LS-S_2 structures, respectively, shown in **a**.

The relative amplitudes of the HS-S_2 and LS-S_2 signals vary under different experimental conditions which indicates that the equilibrium between the HS-S_2 and LS-S_2 states can be perturbed (Zimmermann and Rutherford 1986; Pokhrel and Brudvig 2014; Vinyard et al. 2017; Boussac 2019; Amin et al. 2021). Notably, in spinach PSII, the EPR signal of the HS-S_2 state can be decreased below detection limits by a high concentration of glycerol (Zimmermann and Rutherford 1986; Pokhrel and Brudvig 2014) which is typically used during purification as a stabilizing agent and as a cryoprotectant (Shen et al. 2011; Boussac et al. 2018). Indeed, a 1.90 Å resolution X-ray crystal structure of PSII from the cyanobacteria *Thermosynechococcus vulcanus* (Umena et al. 2011) reports several glycerol molecules bound throughout the structure, but at sites distant to the OEC and unlikely to perturb the mechanism of water oxidation. An independent re-refinement of the same structure data (Wiwczar et al. 2017) reported an additional glycerol

molecule bound at the narrow channel only 11 Å away from the OEC, at a position connected to the OEC by four tightly coupled hydrogen-bonded water molecules (Fig. 1). Importantly, this modeled glycerol replaces a cluster of water molecules found in high-resolution PSII structures, removing hydrogen-bonding partners in the narrow channel (Fig. 1) (Umena et al. 2011; Suga et al. 2015; Tanaka et al. 2017; Kato et al. 2021; Gisriel et al. 2022). Further discussion on this glycerol assignment is provided in the Results and Discussion section. In this study, we address how this glycerol perturbs the relative stability of S_2 state isomers in cyanobacterial PSII. Our study is based on the energetics of quantum mechanics/molecular mechanics (QM/MM) models for HS-S_2 and LS-S_2 states with and without glycerol bound at the narrow channel.

Methods

QM/MM models were built as described (Askerka et al. 2014; Vinyard et al. 2017; Ghosh et al. 2020), constructing the QM layer to include the OEC, one Cl ion, 13 waters, and the side chain of 14 amino acids (D1-D61, D1-S169, D1-D170, D1-G171, D1-N181, D1-E189, D1-H332, D1-E333, D1-H337, D1-D342, D1-A344, CP43-E354, CP43-R357, and D2-K317). Remaining atoms within 15 Å of the OEC are included in the MM layer. The QM/MM structures were optimized using the ONIOM method (Vreven and Morokuma 2000) in Gaussian16 (Frisch et al. 2016) from coordinates provided by Wiwczar et al. (2017, PDB 5V2C) or Umena et al. (2011, PDB 3WU2). The DFT-QM/MM energy calculations were performed using the LanL2DZ pseudopotential and basis set (Hay and Wadt 1985; da Silva Filho et al. 2007) for Mn and Ca atoms and the 6-31G(d) basis set (Hariharan and Pople 1973) for all other atoms. The MM layer was calculated using the AMBER force field (Case et al. 2021). Structure visualization was performed using Coot (version 0.9.7) and PyMOL (version 2.5.1) software packages (Emsley et al. 2010; Schrödinger, LLC 2015). Note that previous versions of Coot calculated cryogenic-electron microscopy (cryo-EM) map contour levels differently than newer versions.

Results and Discussion

Figure 3 shows the optimized structural models, highlighting changes in hydrogen bonding when comparing the HS-S_2 and LS-S_2 states with and without glycerol bound at the narrow channel. In these models, the S_2 state energy is influenced by the hydrogen-bond network of waters W_{X1}, W_{X2}, W_{X3}, W_{X4}, and W_{X5} in the narrow water channel. We identify two main configurations of the hydrogen-bond network (labeled HBN-1 and HBN-2 in Fig. 3).

In HBN-1, a hydrogen bond is established between W_{X1} and D1-Asp61, stabilizing the deprotonated form of D1-Asp61 and orienting donor hydrogen bonds in the narrow channel towards the OEC (Fig. 3). In the HBN-2, the donor hydrogen bonds are flipped, so there is no hydrogen bond between W_{X1} and D1-Asp61 and W_{X4} sacrifices one of its hydrogen bonds by pointing towards a hydrophobic pocket. Thus, the total number of hydrogen bonds in the narrow channel is reduced (Fig. 3). We note that the configuration of hydrogen bonds in the HBN-2, which is missing a hydrogen bond between W_{X1} and D1-Asp61, favors proton transfer from W1 to D1-Asp61 as a result of the high-valent Mn4(IV) decreasing the pK_a of W1 (Fig. 3) (Saito et al. 2020; Ghosh et al. 2020).

Glycerol binding replaces W_{X4} and thus removes the destabilizing effect of the hydrophobic pocket in the glycerol-absent QM/MM model. In addition, glycerol provides a hydrogen-bonding interaction with W_{X3}. Therefore, glycerol significantly perturbs the hydrogen-bond configuration in the narrow channel. Detailed relative energies are found in Table 1. In the LS-S_2 state, proton transfer from W1 to D1-Asp61 is further stabilized upon glycerol binding since

glycerol favors the HBN-2. In contrast, the Mn4(III) in the HS-S_2 state does not stabilize proton transfer from W1 to D1-Asp61 resulting in HBN-1 being favored in the HS-S_2 state when glycerol is bound (Supplemental Fig. 1). Therefore, we find that glycerol binding stabilizes the HBN-2 LS-S_2 state relative to HS-S_2 configuration.

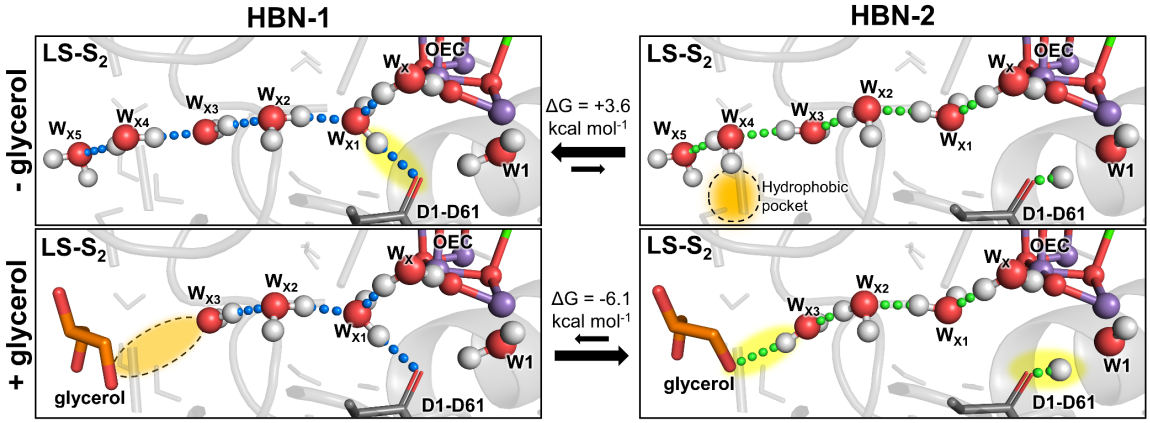

Fig. 3. Comparison of optimized DFT-QM/MM structural models of PSII in the low-spin S_2 state, highlighting changes in hydrogen bonds at the narrow channel induced by glycerol binding. Top panels correspond to structures without glycerol (- glycerol) while lower panels correspond to structures with glycerol (+ glycerol). Left panels correspond to 'hydrogen-bond network 1' (HBN-1), including a hydrogen bond from W_{X1} to D1-Asp61, stabilizing the deprotonated form of D1-Asp61. Right panels correspond to 'hydrogen-bond network 2' (HBN-2), where W_{X1} does not form a hydrogen bond with D1-Asp61, stabilizing the protonated form of D1-Asp61. Notable features which stabilize the HBN are highlighted in yellow while absent/destabilizing features are highlighted in orange and dashed lines. DFT-QM/MM energy differences, shown in kcal mol^{-1}, demonstrate that glycerol binding stabilizes the HBN-2 configuration in the LS-S_2 state.

In summary, the relative energies of low- and high-spin states, with and without glycerol with hydrogen-bond network HBN-1 and HBN-2 (shown in Table 1) indicate that the HS-S_2 and LS-S_2 states without glycerol are nearly isoenergetic with an energy difference of only -0.1 kcal mol^{-1} (Fig. 4). This is consistent with previous results that likewise report near isoenergetic energy levels (Pantazis et al. 2012; Bovi et al. 2013; Vinyard et al. 2017; Boussac et al. 2018). In contrast, the LS-S_2 state with glycerol bound favors HBN-2 and produces an energy difference of +6.5 kcal mol^{-1} compared to the HS-S_2 state with glycerol bound which favors HBN-1 (Fig. 4). Therefore, glycerol's effect on the hydrogen-bond network stabilizes the LS-S_2 state relative to the HS-S_2 isomer.

Table 1 Relative energy calculations of QM/MM optimized models

Structure	Energy Difference (kcal mol^{-1})[a]			
	HBN-1		HBN-2	
	LS-S_2	HS-S_2	LS-S_2	HS-S_2
- glycerol	+0.1	0	+3.7	+12.1
+ glycerol	+6.1	+6.5	0	+14.7

[a]Values are scaled to the lowest energy model per structure.

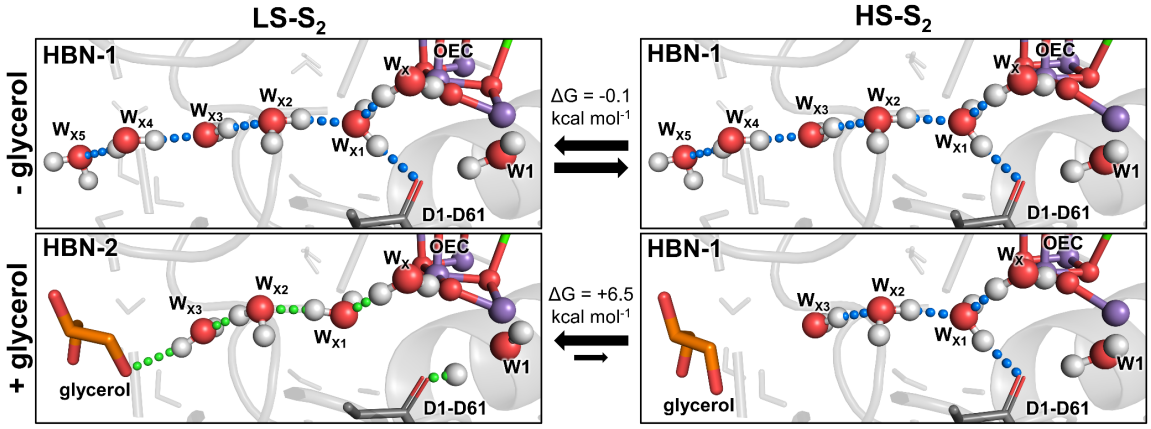

Fig. 4 Optimized DFT-QM/MM structural models of PSII showing the effect of glycerol binding at the narrow water channel on the LS-S_2 and HS-S_2 state equilibrium. Left panels correspond to the LS-S_2 state in the lowest energy HBN configuration. Right panels correspond to the HS-S_2 state in the lowest energy HBN configuration. DFT-QM/MM energy differences are shown in the middle in kcal mol^{-1}. Top panels correspond to structures without glycerol (- glycerol), showing that the LS-S_2 and HS-S_2 states are nearly isoenergetic. Lower panels correspond to structures with glycerol (+ glycerol), showing that glycerol binding significantly stabilizes the LS-S_2 state relative to the HS-S_2 state.

The reported results are consistent with the lack of the HS-S_2 EPR signal from wild-type cyanobacterial PSII (Yachandra et al. 1996; Boussac et al. 2018). A similar perturbation of the hydrogen-bond network may also explain the effect of glycerol on spinach PSII, which shifts the S_2 state equilibrium to favor the LS-S_2 state as observed in spectral amplitude shifts between the HS g = 4.1 signal and the LS g = 2.0 multiline signal (Fig. 2) (Zimmermann and Rutherford 1986). However, an important difference between cyanobacterial and plant type PSII is found in the narrow channel. In cyanobacterial PSII, residue D1-Asn87 hydrogen bonds to W_{X2} in the narrow channel. In comparison, in plant type PSII, the corresponding residue is D1-Ala87, resulting in one fewer hydrogen bond and generating a cavity that likely alters the hydrogen-bond network (Retegan and Pantazis 2017). While the current study identifies how the cyanobacterial hydrogen-bond network can be perturbed by a glycerol molecule, additional studies are required to determine the analogous mechanism in the plant type PSII, which has a modified narrow channel hydrogen-bond network. It is also worth mentioning that while our DFT-QM/MM models are calculated using structural S_2 isomers consistent with models by Pantazis et al. (2012), alternative S_2 isomer models exist (Shoji et al. 2015; Capone et al. 2016; Chatterjee et al. 2019; Corry and O'Malley 2019; Pushkar et al. 2019). Though we did not test those other models, their differences are unlikely to affect our proposed mechanism which implicates the hydrogen-bond network of narrow channel waters and the effect of Mn4 on the pK_a of D1-Asp61. Recently, structures of S_2 and S_3 state enriched PSII have been determined through X-ray free electron laser methods (Kern et al. 2018; Suga et al. 2019; Ibrahim et al. 2020). These have been discussed (Ibrahim et al. 2021; Wang et al. 2021) and used for important computational work on S-state transitions (Yang et al. 2021). However, those structures and subsequent computations do not include W_{X1} on the basis of apparent absence in the experimental density maps of the LS-S_2 state in the absence of glycerol, and thus have disrupted S_2-state hydrogen-bond networks.

In addition to the energetic effects, the reported binding site of glycerol also has implications on the interpretation of the functional role of the narrow channel in water oxidation. There has been discussion that the narrow channel might be a proton egress pathway during

water oxidation (Vogt et al. 2015; Kaur et al. 2021). However, glycerol's binding location in the narrow channel disrupts the otherwise highly coupled water chain, which would be expected to impair efficient proton transport through the hypothesized Grotthuss-type mechanism (Cukierman 2006; Ghosh et al. 2019; Kaur et al. 2021). If the narrow channel is the main proton egress pathway, the binding of glycerol should result in slower oxygen evolution rates. However, this has not been directly experimentally observed despite detailed work on cyanobacterial oxygen-evolution rates (Ghosh et al. 2019), suggesting that the narrow channel is not the primary pathway for proton transfer from the OEC. The narrow channel may instead function as a water-transport pathway or to stabilize the OEC. In the latter role, the narrow channel could provide long-range allostery to affect the water-oxidation rate. Alternatively, it may be possible for the glycerol to be loosely bound and flexibly shift its position, allowing protons or water to pass through the narrow channel unimpeded. However, the electron density does not suggest a loosely bound glycerol, evident by the glycerol's similar B-factor to the nearby protein environment (Wiwczar et al. 2017, PDB 5V2C).

It is also worth reflecting on glycerol's contribution to existing experimental evidence concerning the S_2 state. Here, we find that glycerol bound to the narrow channel is able to influence the OEC energetics by perturbing the narrow channel HBN such that W_{X1} and W1 are affected. Interestingly, both ammonia and methanol have been proposed to bind to the OEC by replacing and/or perturbing these same two water molecules (Askerka et al. 2015; Nagashima and Mino 2017). Furthermore, ammonia and methanol are likewise observed to shift the equilibrium of the S_2 state isomers (Pokhrel and Brudvig 2014). This may result from perturbation of the hydrogen-bond network, similar to our results for glycerol binding. Waters near O4 and Mn4 have also been implicated in mechanisms for early water binding in the S_2 to S_3 transition (Askerka et al. 2016; Siegbahn 2018; Pushkar et al. 2019; Mandal et al. 2021). Also concerning the S_2 to S_3 transition, proposed mechanisms suggest that this transition occurs via the HS-S_2 isomer (Askerka et al. 2015; Retegan et al. 2015). Such a mechanism would result in altered kinetics if the equilibrium between the HS-S_2/LS-S_2 states changes. While we find that glycerol produces shifts in the S_2 isomer equilibrium, we are not aware of detailed experimental evidence to suggest that glycerol alters the oxygen-evolution rates. That observation is consistent with kinetic measurements showing that the S_2 to S_3 transition is not rate limiting (Haumann et al. 2005).

With regard to the additional binding site of glycerol proposed by Wiwczar et al. (2017), several high-resolution structures of cyanobacterial PSII have been determined in recent years. None of the reported structures model glycerol at that binding site (Tanaka et al. 2017; Suga et al. 2017; Kern et al. 2018; Kato et al. 2021; Gisriel et al. 2022). These results open the question as to the frequency of glycerol binding in the PSII structures and the EPR data. Upon close examination of previous literature, it becomes difficult to either validate or invalidate the presence of glycerol in any given study. Regarding the EPR literature, the precise methods used during sample preparation are not always provided and/or lack necessary details. Concerning the PSII structures, which explicitly use glycerol during sample preparation, there are consistently structural features at the proposed glycerol binding location, but — as was the case in the original Umena et al. (2011) structure — these features are modeled as water molecules (Fig. 5). Furthermore, while glycerol is used during purification, recent structural studies often exclude glycerol from the final crystal/cryo-EM buffer solution. Interestingly, several high-resolution structures that include glycerol in the final crystallization solution modeled glycerol throughout the structure, whereas other structures that exclude glycerol in the final crystallization/cryo-EM solution had no modeled glycerol molecules (Fig. 5). However, it is often difficult to differentiate

between a glycerol molecule and a small cluster of water molecules in a structural map, adding additional uncertainty. All we can currently say is that, in a variety of structural, biochemical, and biophysical studies, when methods of sufficient detail are provided, a glycerol solution is typically used in at least one step of sample preparation (Boussac et al. 1998; Shen et al. 2011; Debus 2014; Pokhrel and Brudvig 2014; Tanaka et al. 2017; Suga et al. 2017; Kern et al. 2018; Kato et al. 2021).

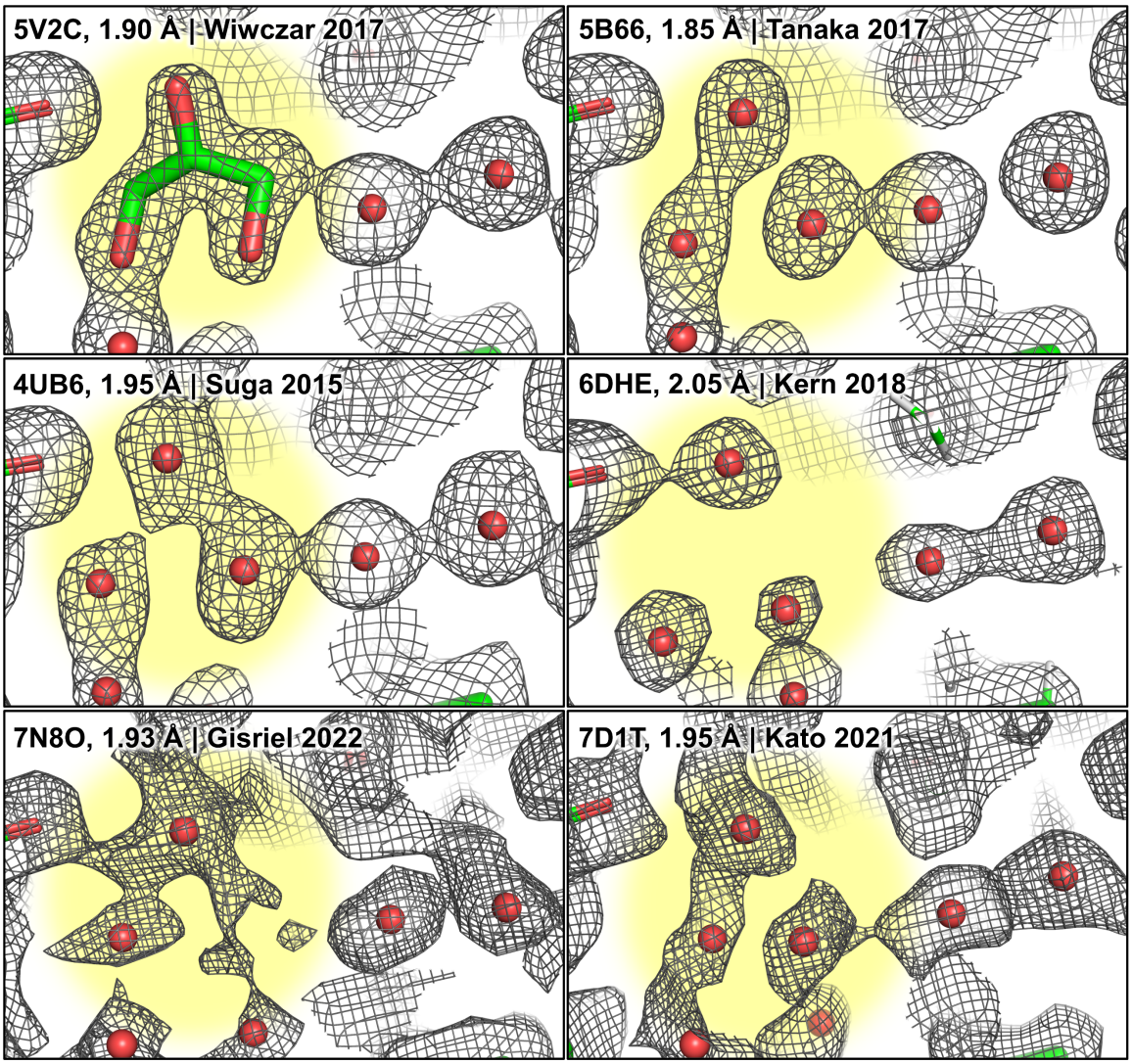

Fig. 5 Visualization of recent high-resolution structures of PSII with evidence for glycerol binding. Map and models for each structure are shown and oriented to observe the glycerol binding site proposed by Wiwczar et al. (2017). The equivalent glycerol binding site is highlighted in yellow. Each subfigure is labeled with the PDB accession code, reported global resolution, and first author. Depicted structures that exclude glycerol in the final crystal/cryo-EM buffer solution are 5B66, 6DHE, 7N8O, and 7D1T. The grey mesh represents the structure map contoured at 0.5σ and the mesh density has been increased to assist in visualization. Note that, for the cryo-EM structures 7N8O and 7D1T, the equivalent contour level calculated using older Coot versions is ~2σ. Modeled waters are depicted using red spheres.

In conclusion, we find that the binding of glycerol in cyanobacterial PSII reported by (Wiwczar et al. 2017) perturbs the hydrogen-bond network in the narrow water channel which stabilizes the LS-S_2 state of the OEC with protonated D1-Asp61, relative to the HS-S_2 state where D1-Asp61 is deprotonated (Fig. 3 and 4). DFT-QM/MM calculations suggest that the energy difference between the HS-S_2 and LS-S_2 states increases to +6.5 kcal mol^{-1} when glycerol is bound, which is significantly higher than the almost isoenergetic energy of the HS-S_2 and LS-S_2 states when glycerol is not bound (Fig. 4 and Table 1). Further, the binding of glycerol at the narrow water channel has implications on our understanding of PSII function since it regulates the relative stability of OEC catalytic intermediates that are essential for water oxidation.

References

Amin M, Kaur D, Gunner MR, Brudvig G (2021) Toward understanding the S_2-S_3 transition in the Kok cycle of Photosystem II: Lessons from Sr-substituted structure. Inorganic Chemistry Communications 133:108890. https://doi.org/10.1016/j.inoche.2021.108890

Askerka M, Vinyard DJ, Brudvig GW, Batista VS (2015) NH_3 binding to the S_2 state of the O_2-evolving complex of photosystem II: Analogue to H_2O binding during the $S_2 \rightarrow S_3$ transition. Biochemistry 54:5783–5786. https://doi.org/10.1021/acs.biochem.5b00974

Askerka M, Wang J, Brudvig GW, Batista VS (2014) Structural changes in the oxygen-evolving complex of photosystem II induced by the S_1 to S_2 transition: A combined XRD and QM/MM study. Biochemistry 53:6860–6862. https://doi.org/10.1021/bi5011915

Askerka M, Wang J, Vinyard DJ, et al (2016) S_3 state of the O_2-evolving complex of photosystem II: Insights from QM/MM, EXAFS, and femtosecond X-ray diffraction. Biochemistry 55:981–984. https://doi.org/10.1021/acs.biochem.6b00041

Blankenship RE (2021) Molecular Mechanisms of Photosynthesis, 3rd Edition. John Wiley & Sons

Boussac A (2019) Temperature dependence of the high-spin S_2 to S_3 transition in Photosystem II: Mechanistic consequences. Biochim Biophys Acta (BBA) - Bioenergetics 1860:508–518. https://doi.org/10.1016/j.bbabio.2019.05.001

Boussac A, Kuhl H, Un S, et al (1998) Effect of near-infrared light on the S_2-state of the manganese complex of Photosystem II from *Synechococcus elongatus*. Biochemistry 37:8995–9000. https://doi.org/10.1021/bi980195b

Boussac A, Rutherford AW, Sugiura M (2015) Electron transfer pathways from the S_2-states to the S_3-states either after a Ca^{2+}/Sr^{2+} or a Cl^-/I^- exchange in Photosystem II from *Thermosynechococcus elongatus*. Biochim Biophys Acta (BBA) - Bioenergetics 1847:576–586. https://doi.org/10.1016/j.bbabio.2015.03.006

Boussac A, Ugur I, Marion A, et al (2018) The low spin - high spin equilibrium in the S_2-state of the water oxidizing enzyme. Biochim Biophys Acta (BBA) - Bioenergetics 1859:342–356. https://doi.org/10.1016/j.bbabio.2018.02.010

Bovi D, Narzi D, Guidoni L (2013) The S_2 state of the oxygen-evolving complex of Photosystem II explored by QM/MM dynamics: Spin surfaces and metastable states suggest a

reaction path towards the S_3 state. Angew Chem Int Ed 52:11744–11749. https://doi.org/10.1002/anie.201306667

Brudvig GW, Casey JL, Sauer K (1983) The effect of temperature on the formation and decay of the multiline EPR signal species associated with photosynthetic oxygen evolution. Biochim Biophys Acta (BBA) - Bioenergetics 723:366–371. https://doi.org/10.1016/0005-2728(83)90042-7

Capone M, Narzi D, Bovi D, Guidoni L (2016) Mechanism of Water Delivery to the Active Site of Photosystem II along the S_2 to S_3 Transition. J Phys Chem Lett 7:592–596. https://doi.org/10.1021/acs.jpclett.5b02851

Case DA, Aktulga HM, Belfon K, et al (2021) AMBER 2021. University of California, San Francisco

Chatterjee R, Lassalle L, Gul S, et al (2019) Structural isomers of the S_2 state in photosystem II: do they exist at room temperature and are they important for function? Physiologia Plantarum 166:60–72. https://doi.org/10.1111/ppl.12947

Corry TA, O'Malley PJ (2019) Proton Isomers Rationalize the High- and Low-Spin Forms of the S_2 State Intermediate in the Water-Oxidizing Reaction of Photosystem II. J Phys Chem Lett 10:5226–5230. https://doi.org/10.1021/acs.jpclett.9b01372

Cukierman S (2006) Et tu, Grotthuss! and other unfinished stories. Biochimica et Biophysica Acta (BBA) - Bioenergetics 1757:876–885. https://doi.org/10.1016/j.bbabio.2005.12.001

da Silva Filho DA, Coropceanu V, Fichou D, et al (2007) Hole-vibronic coupling in oligothiophenes: Impact of backbone torsional flexibility on relaxation energies. Phil Trans R Soc A 365:1435–1452. https://doi.org/10.1098/rsta.2007.2025

Debus RJ (2014) Evidence from FTIR Difference Spectroscopy That D1-Asp61 Influences the Water Reactions of the Oxygen-Evolving Mn_4CaO_5 Cluster of Photosystem II. Biochemistry 53:2941–2955. https://doi.org/10.1021/bi500309f

Dismukes GC, Siderer Y (1980) EPR spectroscopic observations of a manganese center associated with water oxidation in spinach chloroplasts. FEBS Letters 121:78–80. https://doi.org/10.1016/0014-5793(80)81270-1

Emsley P, Lohkamp B, Scott WG, Cowtan K (2010) Features and development of Coot. Acta Cryst D 66:486–501. https://doi.org/10.1107/S0907444910007493

Frisch MJ, Trucks GW, Schlegel HB, et al (2016) Gaussian 16 Rev. C.01. Gaussian, Inc., Wallingford CT

Ghosh I, Banerjee G, Reiss K, et al (2020) D1-S169A substitution of photosystem II reveals a novel S_2-state structure. Biochim Biophys Acta (BBA) - Bioenergetics 1861:148301. https://doi.org/10.1016/j.bbabio.2020.148301

Ghosh I, Khan S, Banerjee G, et al (2019) Insights into Proton-Transfer Pathways during Water Oxidation in Photosystem II. J Phys Chem B 123:8195–8202. https://doi.org/10.1021/acs.jpcb.9b06244

Gisriel CJ, Wang J, Liu J, et al (2022) High-resolution cryo-electron microscopy structure of photosystem II from the mesophilic cyanobacterium, *Synechocystis* sp. PCC 6803. PNAS 119:. https://doi.org/10.1073/pnas.2116765118

Hariharan PC, Pople JA (1973) The influence of polarization functions on molecular orbital hydrogenation energies. Theoret Chim Acta 28:213–222. https://doi.org/10.1007/BF00533485

Haumann M, Liebisch P, Müller C, et al (2005) Photosynthetic O_2 Formation Tracked by Time-Resolved X-ray Experiments. Science 310:1019–1021. https://doi.org/10.1126/science.1117551

Hay PJ, Wadt WR (1985) Ab initio effective core potentials for molecular calculations. Potentials for K to Au including the outermost core orbitals. J Chem Phys 82:299–310. https://doi.org/10.1063/1.448975

Hillier W, Wydrzynski T (2000) The affinities for the two substrate water binding sites in the O_2 evolving complex of photosystem II vary independently during S-state turnover. Biochemistry 39:4399–4405. https://doi.org/10.1021/bi992318d

Ibrahim M, Fransson T, Chatterjee R, et al (2020) Untangling the sequence of events during the $S_2 \rightarrow S_3$ transition in photosystem II and implications for the water oxidation mechanism. PNAS 117:12624–12635. https://doi.org/10.1073/pnas.2000529117

Ibrahim M, Moriarty NW, Kern J, et al (2021) Reply to Wang et al.: Clear evidence of binding of Ox to the oxygen-evolving complex of photosystem II is best observed in the omit map. PNAS 118:. https://doi.org/10.1073/pnas.2102342118

Kato K, Miyazaki N, Hamaguchi T, et al (2021) High-resolution cryo-EM structure of photosystem II reveals damage from high-dose electron beams. Communications Biology 4:1–11. https://doi.org/10.1038/s42003-021-01919-3

Kaur D, Zhang Y, Reiss KM, et al (2021) Proton exit pathways surrounding the oxygen evolving complex of photosystem II. Biochim Biophys Acta (BBA) - Bioenergetics 1862:148446. https://doi.org/10.1016/j.bbabio.2021.148446

Kern J, Chatterjee R, Young ID, et al (2018) Structures of the intermediates of Kok's photosynthetic water oxidation clock. Nature 563:421. https://doi.org/10.1038/s41586-018-0681-2

Kok B, Forbush B, McGloin M (1970) Cooperation of charges in photosynthetic O_2 evolution–I. a linear four step mechanism. Photochem Photobiol 11:457–475. https://doi.org/10.1111/j.1751-1097.1970.tb06017.x

Mandal M, Saito K, Ishikita H (2021) Requirement of Chloride for the Downhill Electron Transfer Pathway from the Water-Splitting Center in Natural Photosynthesis. J Phys Chem B. https://doi.org/10.1021/acs.jpcb.1c09176

Nagashima H, Mino H (2017) Location of methanol on the S_2 state Mn cluster in Photosystem II studied by proton matrix electron nuclear double resonance. J Phys Chem Lett 8:621–625. https://doi.org/10.1021/acs.jpclett.7b00110

Pantazis DA, Ames W, Cox N, et al (2012) Two interconvertible structures that explain the spectroscopic properties of the oxygen-evolving complex of Photosystem II in the S_2 state. Angew Chem Int Ed 51:9935–9940. https://doi.org/10.1002/anie.201204705

Pokhrel R, Brudvig GW (2014) Oxygen-evolving complex of photosystem II: Correlating structure with spectroscopy. Phys Chem Chem Phys 16:11812–11821. https://doi.org/10.1039/C4CP00493K

Pushkar Y, K. Ravari A, Jensen SC, Palenik M (2019) Early binding of substrate oxygen is responsible for a spectroscopically distinct S_2 state in Photosystem II. J Phys Chem Lett 10:5284–5291. https://doi.org/10.1021/acs.jpclett.9b01255

Retegan M, Krewald V, Mamedov F, et al (2015) A five-coordinate Mn(IV) intermediate in biological water oxidation: Spectroscopic signature and a pivot mechanism for water binding. Chem Sci 7:72–84. https://doi.org/10.1039/C5SC03124A

Retegan M, Pantazis DA (2017) Differences in the Active Site of Water Oxidation among Photosynthetic Organisms. J Am Chem Soc 139:14340–14343. https://doi.org/10.1021/jacs.7b06351

Saito K, Nakagawa M, Ishikita H (2020) pKa of the ligand water molecules in the oxygen-evolving Mn_4CaO_5 cluster in photosystem II. Commun Chem 3:1–7. https://doi.org/10.1038/s42004-020-00336-7

Schrödinger, LLC (2015) The PyMOL Molecular Graphics System, Version 2.5.1

Shen J-R (2015) The structure of photosystem II and the mechanism of water oxidation in photosynthesis. Annu Rev Plant Biol 66:23–48. https://doi.org/10.1146/annurev-arplant-050312-120129

Shen J-R, Kawakami K, Koike H (2011) Purification and Crystallization of Oxygen-Evolving Photosystem II Core Complex from Thermophilic Cyanobacteria. In: Carpentier R (ed) Photosynthesis Research Protocols. Humana Press, Totowa, NJ, pp 41–51

Shoji M, Isobe H, Yamaguchi K (2015) QM/MM study of the S_2 to S_3 transition reaction in the oxygen-evolving complex of photosystem II. Chemical Physics Letters 636:172–179. https://doi.org/10.1016/j.cplett.2015.07.039

Siegbahn PEM (2018) The S_2 to S_3 transition for water oxidation in PSII (photosystem II), revisited. Phys Chem Chem Phys 20:22926–22931. https://doi.org/10.1039/C8CP03720E

Sproviero EM, Shinopoulos K, Gascón JA, et al (2008) QM/MM computational studies of substrate water binding to the oxygen-evolving centre of photosystem II. Phil Trans R Soc B 363:1149–1156. https://doi.org/10.1098/rstb.2007.2210

Suga M, Akita F, Hirata K, et al (2015) Native structure of photosystem II at 1.95 Å resolution viewed by femtosecond X-ray pulses. Nature 517:99–103. https://doi.org/10.1038/nature13991

Suga M, Akita F, Sugahara M, et al (2017) Light-induced structural changes and the site of O=O bond formation in PSII caught by XFEL. Nature 543:131–135. https://doi.org/10.1038/nature21400

Suga M, Akita F, Yamashita K, et al (2019) An oxyl/oxo mechanism for oxygen-oxygen coupling in PSII revealed by an x-ray free-electron laser. Science. https://doi.org/10.1126/science.aax6998

Takaoka T, Sakashita N, Saito K, Ishikita H (2016) pKa of a Proton-Conducting Water Chain in Photosystem II. J Phys Chem Lett 7:1925–1932. https://doi.org/10.1021/acs.jpclett.6b00656

Tanaka A, Fukushima Y, Kamiya N (2017) Two Different Structures of the Oxygen-Evolving Complex in the Same Polypeptide Frameworks of Photosystem II. J Am Chem Soc 139:1718–1721. https://doi.org/10.1021/jacs.6b09666

Umena Y, Kawakami K, Shen J-R, Kamiya N (2011) Crystal structure of oxygen-evolving photosystem II at a resolution of 1.9 Å. Nature 473:55–60. https://doi.org/10.1038/nature09913

Vinyard DJ, Brudvig GW (2017) Progress toward a molecular mechanism of water oxidation in photosystem II. Annu Rev Phys Chem 68:101–116. https://doi.org/10.1146/annurev-physchem-052516-044820

Vinyard DJ, Khan S, Askerka M, et al (2017) Energetics of the S_2 state spin isomers of the oxygen-evolving complex of Photosystem II. J Phys Chem B 121:1020–1025. https://doi.org/10.1021/acs.jpcb.7b00110

Vogt L, Vinyard DJ, Khan S, Brudvig GW (2015) Oxygen-evolving complex of Photosystem II: An analysis of second-shell residues and hydrogen-bonding networks. Curr Opin Chem Biol 25:152–158. https://doi.org/10.1016/j.cbpa.2014.12.040

Vreven T, Morokuma K (2000) The ONIOM (our own N-layered integrated molecular orbital + molecular mechanics) method for the first singlet excited (S1) state photoisomerization path of a retinal protonated Schiff base. J Chem Phys 113:2969–2975. https://doi.org/10.1063/1.1287059

Wang J, Armstrong WH, Batista VS (2021) Do crystallographic XFEL data support binding of a water molecule to the oxygen-evolving complex of photosystem II exposed to two flashes of light? PNAS 118:. https://doi.org/10.1073/pnas.2023982118

Wiwczar JM, LaFountain AM, Wang J, et al (2017) Chlorophyll *a* with a farnesyl tail in thermophilic cyanobacteria. Photosynth Res 134:175–182. https://doi.org/10.1007/s11120-017-0425-4

Yachandra VK, Sauer K, Klein MP (1996) Manganese Cluster in Photosynthesis: Where Plants Oxidize Water to Dioxygen. Chem Rev 96:2927–2950. https://doi.org/10.1021/cr950052k

Yang KR, Lakshmi KV, Brudvig GW, Batista VS (2021) Is Deprotonation of the Oxygen-Evolving Complex of Photosystem II during the $S_1 \rightarrow S_2$ Transition Suppressed by Proton

Quantum Delocalization? J Am Chem Soc 143:8324–8332. https://doi.org/10.1021/jacs.1c00633

Zimmermann JL, Rutherford AW (1984) EPR studies of the oxygen-evolving enzyme of Photosystem II. Biochim Biophys Acta (BBA) - Bioenergetics 767:160–167. https://doi.org/10.1016/0005-2728(84)90091-4

Zimmermann JL, Rutherford AW (1986) Electron paramagnetic resonance properties of the S_2 state of the oxygen-evolving complex of photosystem II. Biochemistry 25:4609–4615. https://doi.org/10.1021/bi00364a023

Declarations

Funding:

This work was supported by Department of Energy, Office of Basic Energy Sciences, Division of Chemical Sciences grant DE-FG02-05ER15646 to G.W.B.

Conflicts of interest:

The authors declare no competing interests.

Author contributions:

All authors contributed to discussion and edits of the manuscript. D.A.F. and J.W. performed structural analysis. K.R., J.L, K.R.Y., and M.A. calculated QM/MM models. D.A.F. and J.M.W. led manuscript preparation.

Availability of data and material:

The model coordinates are included as supplemental data files.